

New theoretical results for a bidimensional quasi-adiabatic model of muon-catalyzed fusion

Francisco Caruso^{a,b}, Vitor Oguri^b, Felipe Silveira^b & Amos Troper^a

^a *Centro Brasileiro de Pesquisas Físicas, Rio de Janeiro, Brazil.*

^b *Universidade do Estado do Rio de Janeiro, Rio de Janeiro, Brazil.*

Abstract

The ground state energy, its respective eigenfunction and some specific parameters of ionized muonic molecules formed by proton-proton, deuterium-deuterium and tritium-tritium nuclei plus a negative muon confined in a two-dimensional spatial region are calculated. A 2D Coulombic potential of the type $\ln(r)$ is considered for the electrostatic interaction, instead of the usual 3D $1/r$ potential. The two-dimensional effective potentials of these three-body molecules are analytically calculated within a quasi-adiabatic approximation. Then, the resulting Schrödinger equation is numerically solved for each kind of molecule with a slightly modified Numerov method. The results are confronted with those got for the same molecules in 3D and 2D, in both cases adopting the $1/r$ Ansatz. On the one hand, these comparisons put in evidence that the choice of the potential energy significantly influences the nuclear fusion probability. In particular, we find, for the $tt\mu$ molecule, that this probability is 10^9 times greater using the two-dimensional $\ln(r)$ Coulombic potential compared to the prediction in three-dimensions with the $1/r$ potential. In addition, for this same molecule, the tunnelling ratio is 2×10^4 greater than in 3D. On the other hand, all these results put in evidence also the distinguished role of the “centrifugal potential” in the 2D effective potential, showing that the geometrical nature of planar space plays a quite relevant role for the improvement of fusion rates in 2D.

Keywords:

muon physics, muonic molecule, muon-catalyzed fusion, planar physics, quantum physics

1. Introduction

The general idea that a particular mechanism of nuclear fusion can be related to muon physics is a good example of a physical process proposed for a specific explanation which, as time goes on, acquire *per se* a major intrinsic interest, opening therefore a new promising research field: the search for sustainable energy production through cold fusion catalyzed by muon captures.

In 1947, Lattes, Occhialini and Powell, discovered the pion, π^- , from cosmic rays. Stopped in the photo-emulsion it gives rise to a muon and an antineutrino [1]. Historically, Frank [2] proposed that the μ had a probability of been captured by deuterons (d) presented in the photo-emulsion, originating a $d\mu$ atom. Like neutrons, these atoms could go through matter and can easily go inside molecules. If it reaches a close distance to a proton, one might observe the following fusion reaction: $d\mu + p \rightarrow {}^3\text{He} + \mu + 5.5 \text{ MeV}$ [2].

In 1948, Sakharov suggested a fusion mechanism from the nuclear reaction produced in liquid deuterium, $d + d\mu \rightarrow {}^4\text{He} + \mu$ [3]. Due to the fact that the μ is 200 heavier than the electron, this makes the nuclei of this new molecule much closer than when they were formed by an electron ($\simeq 500 \text{ fm}$ in this case), thus increasing the probability of the nuclei to fuse [4, 5].

From the experimental point of view, the first muon catalyzed fusion was observed by chance by Alvarez and collaborators [6]. Just in 1973, Matveenko [7] and Ponomarev [8] developed a high-precision numerical method for the description of a three-body Coulombic system.

The muon catalysed fusion (μCF) is currently considered as an effective and reliable way of achieving a sustainable low temperature nuclear fusion process [4, 9, 10]. Little progress has been made in recent past years, since the same old objection still holds on: on the one hand muon production requires a considerable amount of energy, on the other hand the up to now estimated rates for each individual fusion process are still relatively small, so that the whole process is argued not to be profitable, considered the muon-life-time [11]. In any case, there are many attempts to improve the energy efficiency of this process [12, 13, 14, 15, 16, 17], including a good perspective using a new type of laser-driven muon generator [18]. Some review articles might be useful [5, 9, 10, 19, 20, 21].

The general scope of this article is to shed light on the above objection. In particular, we start from a different approach, focusing on the systematic

calculation of the elementary processes involved in the muon-catalyzed nuclear fusion choosing the electrostatic $\ln(r)$ potential. This means that, in this paper, the following effects on the μ CF are not taken into account: the influence of temperature [12, 13, 14, 22, 23]; the probability of muon sticking the produced helium [24, 25]; and the possibility of target-density effects [26, 27].

In this paper, first of all, we want to investigate the influence of the space dimensionality of the system on the fusion probability. In what sense the probability of fusion could vary by going from a 3D to a 2D molecular model? Can one improve the fusion rate by considering a strictly planar system?

Before going on, it is relevant to stress that, over the recent past years, planar Physics and truly two-dimensional systems have attracted a great deal of attention in connection with graphene [28, 29, 30], and with Quantum Hall Effect [31, 32]. All these quantum systems point to consider that the correct Coulomb inter-electronic potential should be the $\ln(r)$ potential [33], rather than assuming the validity of the usual 3D-dependence in planar systems, corresponding to the $1/r$ potential [34, 35].

Turning back to the scope of our paper, first of all, we need to consider a two-dimensional model of muon-catalyzed fusion. Moreover, even considering a 2D configuration, we must investigate the influence of the Ansatz for the electric potential, which could be of the type $1/r$ or $\ln(r)$ [36], on the fusion rate. This kind of dependence in another planar system (quantum dots) was recently investigated and discussed in two papers [37, 38].

Secondly, instead of giving rough estimates, the model developed here is straightforwardly solved as a quantum mechanical problem. In this sense, we made an effort to obtain an analytical expression for the effective interaction potential between the two molecular nuclei that appears in the Schrödinger equation describing the model of the three-body muonic molecule. The final planar dynamical equation will be solved by using Numerov's numerical method [39, 40], which allows us to determine the $\ell = 0$ wave functions, which deserves special attention as will be clear throughout the paper. In such case, all the predicted probabilities of fusion for different molecules, as well as the tunnelling coefficients for one of the molecular nucleus, are actually computed and not estimated as in all previous papers [11].

A 2D model of the muonic molecule is constructed in Section 2 adopting a quasi-adiabatic approximation, *i.e.*, considering that the movement of the

nucleus is much slower than that of the muon. All the analytical calculations of this model are presented in Section 3. The numerical results are given in Section 4 and the concluding remarks, in Section 5.

2. A two-dimensional model for μCF

The time-independent two dimensional Schrödinger equation which describes a three-body quantum system formed by two positive nuclei (in this work we will use proton, deuteron or triton) and one negative particle (electron or muon) orbiting them is:

$$\left[-\frac{\hbar^2}{2m_1}\nabla_1^2 - \frac{\hbar^2}{2m_2}\nabla_2^2 - \frac{\hbar^2}{2m_3}\nabla_3^2 + V(\vec{r}_{13}, \vec{r}_{23}, \vec{r}_{12}) \right] \Psi(\vec{r}_{13}, \vec{r}_{23}, \vec{r}_{12}) = E_T \Psi(\vec{r}_{13}, \vec{r}_{23}, \vec{r}_{12}) \quad (1)$$

with 1 and 2 being the indices of the two positive nuclei and 3 denotes the negative particle, $\vec{r}_{13} = \vec{r}_3 - \vec{r}_1$, $\vec{r}_{23} = \vec{r}_3 - \vec{r}_2$ and $\vec{r}_{12} = \vec{r}_2 - \vec{r}_1$. The 2D Coulombic potential of mutual interactions is

$$V(\vec{r}_{13}, \vec{r}_{23}, \vec{r}_{12}) = V_0 \ln \frac{r_{13}}{r_0} + V_0 \ln \frac{r_{23}}{r_0} - V_0 \ln \frac{r_{12}}{r_0} \quad (2)$$

which has the advantage of ensuring, at least at the classical level, the electric charge (e) conservation.

In a quasi-adiabatic model, the muon is assumed to follow adiabatically the movement of the two nuclei until the fusion occurs [41, 42]. In this way one can consider that, for the muon, the two nuclei are at fixed positions. Thus, neglecting the two first kinetic terms of Eq. (1), the Schrödinger equation that describes the motion of the muonic part of the molecule:

$$\left[-\frac{\hbar^2}{2m_3}\nabla_3^2 + V_0 \ln \frac{r_{13}}{r_0} + V_0 \ln \frac{r_{23}}{r_0} \right] \Psi(\vec{r}_{13}, \vec{r}_{23}) = E \Psi(\vec{r}_{13}, \vec{r}_{23}) \quad (3)$$

As in 3D model of μCF , another approximation will be made in which one consider that the wave function of the molecule is composed by the sum of the wave functions of the two hydrogen-like atoms, $\psi_{\pm} = N_{\pm}(\psi_a \pm \psi_b)$; one composed by the first nucleus and the muon, ψ_a , and the other, ψ_b , composed by the second nucleus and the (same) muon [41].

We are now able to find the expectation value of the energy of Eq. (3) in the states ψ_{\pm} , which will be denoted W_{\pm} , following the notation of [41]:

$$W_{\pm} = E_0 + \frac{\mathcal{D} \pm \mathcal{E}}{1 \pm \Delta} \quad (4)$$

where E_0 is the ground state energy of the respective atom. Its value depends on the kind of atom we are considering ($p\mu$, $d\mu$, or $t\mu$).

The factors \mathcal{D} and \mathcal{E} to be calculated are the *direct integral* and *exchange integral*, respectively, defined by the integrals:

$$\mathcal{D} = \int \left(\ln(\rho_b)\psi_a^2 + \ln(\rho_a)\psi_b^2 \right) d^{2D}V \quad (5)$$

$$\mathcal{E} = \int \left(\ln(\rho_a)\psi_a\psi_b + \ln(\rho_b)\psi_a\psi_b \right) d^{2D}V \quad (6)$$

and the normalizing factor (called the *overlap integral* Δ) is

$$1 \pm \Delta = \frac{|N_{\pm}|^{-2}}{2} = \int \left(|\psi_a|^2 + |\psi_b|^2 \pm 2\psi_a\psi_b \right) d^{2D}V \quad (7)$$

where we have denoted $r_a = r_{13}$, $r_b = r_{23}$, $\rho_a = r_a/a_0^*$ e $\rho_b = r_b/a_0^*$, with $a_0^* \simeq a_0/206$ being the modified Bohr's radius.

In Eq. (1), we can substitute the muonic part given by the left-hand side of Eq. (3) by the expectation value of the energy W_{\pm} , Eq. (4). This leads to the following dimensionless radial Schrödinger equation for the relative motion of the two nuclei:

$$\left\{ \frac{d^2}{d\rho^2} + \varepsilon - V_{\text{eff}} \right\} u(\rho) = 0 \quad (8)$$

with

$$\psi(\rho, \theta) = \frac{u(\rho)}{\sqrt{\rho}} e^{\pm i\ell\theta}$$

and

$$V_{\text{eff}} = -\frac{\mu}{m_3} [-\ln \rho + W_{\pm}] + \frac{(\ell^2 - \frac{1}{4})}{\rho^2} \quad (9)$$

Here μ is the reduced mass of the two nuclei and m_3 the mass of the muon or the electron. Insofar we are treating muonic molecules, notice that the dimensionless parameter ε is given by $E_T/(e^2/2a_0^*)$. This equation describes, in general, any molecule composed of two positive nuclei of the same type and just one negative particle orbiting them. In this paper, for simplicity, the focus is on the $pp\mu$, $dd\mu$ and $tt\mu$ molecules. We hope to investigate other molecules with different nuclei, like $dt\mu$ in another publication.

The different values of the μ/m_3 factor for each type of molecule involved in the forthcoming calculations are given in the Table 1.

Table 1: Values of the ratio μ/m_3 corresponding to different molecules

Molecule	μ/m_3
<i>ppe</i>	918.0763
<i>dde</i>	1835.2415
<i>ppμ</i>	4.4401
<i>ddμ</i>	8.8758
<i>ttμ</i>	13.2925

3. Analytical calculations

Once in our model the wave function of the muonic molecule is assumed to be formed by the sum of two wave functions of two hydrogen-like atoms (ψ_a, ψ_b), the first thing we need is to determine them in 2D. Therefore, we will start solving the Schrödinger equation for hydrogen like atom in two dimensions given by:

$$\left[-\frac{\hbar^2}{2m_1} \vec{\nabla}_1^2 - \frac{\hbar^2}{2m_2} \vec{\nabla}_2^2 + V(\vec{r}_1, \vec{r}_2) \right] \Psi(\vec{r}_1, \vec{r}_2) = E_T \Psi(\vec{r}_1, \vec{r}_2) \quad (10)$$

with the 2D Coulombic potential of interaction being

$$V(r) = V_0 \ln \left(\frac{|r|}{L} \right)$$

From Eq. (10), it is straightforward to write the radial Schrödinger equation for this atom, in dimensionless units (ρ), as

$$\frac{d^2 u(\rho)}{d\rho^2} + \left[E_0 - \ln(\rho) - \frac{(\ell^2 - \frac{1}{4})}{\rho^2} \right] u(\rho) = 0 \quad (11)$$

Numerical solutions for the ground state energy and wave function of Eq. (11) were obtained by using the Numerov method. The resulting ground state energies E_0 for different molecules are given in Table 2.

Table 2: E_0 values corresponding to different atoms; the value corresponding to the atom composed by an electron is in Rydberg unit, although those values for muonic atoms are shown in modified Rydberg units, $Ry^* \simeq Ry/206$

Atom	E_0
pe	$0.7103 Ry$
de	$0.7103 Ry$
$d\mu$	$0.7503 Ry^*$
$p\mu$	$0.7903 Ry^*$
$t\mu$	$0.7370 Ry^*$

The ground state wave function, obtained by numerically solving Eq. (11) with the Numerov method, is plotted as a continuous line in Fig. 1.

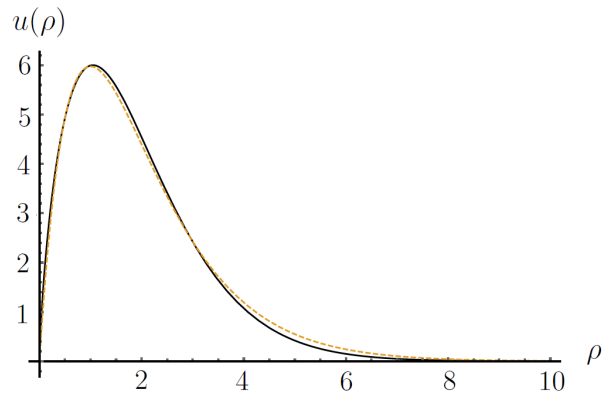


Figure 1: The continuous line show the numerical solution of Eq. (11) for the ground state wave function of hydrogen atom in 2D, and the dashed one is the interpolated function, given by Eq. (12).

In order to get analytical results, this wave function can be well approximated by the following equation, which is represented by the dashed line in Fig. 1.

$$u(\rho) = 120\rho e^{-(\rho+2)} \quad (12)$$

Within this interpolation, the wave functions ψ_a and ψ_b of the two hydrogen atoms can be written, in terms of $u(\rho)$, as

$$\psi_a(\rho) = \frac{120}{e^2} \sqrt{\rho_a} e^{-\rho_a} \quad ; \quad \psi_b(\rho) = \frac{120}{e^2} \sqrt{\rho_b} e^{-\rho_b} \quad (13)$$

where we have used the well known relation $\psi(\rho) = u(\rho)/\sqrt{\rho}$ in 2D. The normalized wave functions are then given by

$$\psi_a(\rho) = \sqrt{\frac{2}{\pi}} \sqrt{\rho_a} e^{-\rho_a} \quad ; \quad \psi_b(\rho) = \sqrt{\frac{2}{\pi}} \sqrt{\rho_b} e^{-\rho_b}$$

Before we can solve Eq. (8), we need to compute the W_{\pm} expression, by solving the three integrals given by Eqs. (5, 6, 7). To do this it is appropriate, as in Ref. [41], to introduce the prolate coordinate system, namely

$$\frac{\rho_a + \rho_b}{R/a_0^*} = \xi \quad ; \quad \frac{\rho_a - \rho_b}{R/a_0^*} = \eta$$

with $1 \leq \xi < \infty$ and $-1 \leq \eta \leq +1$. Denoting $\rho \equiv R/a_0^*$, in this coordinate system, the two-dimensional volume element ($d^{2D}V$) can be written as

$$d^{2D}V = \frac{\rho^2}{4} \frac{(\xi^2 - \eta^2) d\xi d\eta}{\sqrt{(\xi^2 - 1)(1 - \eta^2)}} \quad (14)$$

Once these new coordinates are introduced, we are ready to compute all the integrals in Eqs. (5), (6) and (7). From now on, unless differently stated, all the numerical integrations were made by using the software *Mathematica*, version 11.3.

Let's start by solving Eq. (7). The first two integrals of $|\psi_a|^2$ and $|\psi_b|^2$ are equal to 1, since these wave functions are normalized. So, rewriting Eq. (7) in the prolate coordinate system, we get:

$$\Delta = \frac{\rho^3}{2\pi} \int_{-1}^1 \frac{d\eta}{\sqrt{1 - \eta^2}} \int_1^{\infty} \frac{(\xi^2 - \eta^2)^{\frac{3}{2}} e^{-\xi\rho}}{\sqrt{\xi^2 - 1}} d\xi \quad (15)$$

To solve the integral in $d\xi$, we expanded it up to $\mathcal{O}(\eta^7)$, using

$$(\xi^2 - \eta^2)^{\frac{3}{2}} \simeq \xi^3 - \frac{3}{2}\xi\eta^2 + \frac{3}{8}\frac{\eta^4}{\xi} + \frac{1}{16}\frac{\eta^6}{\xi^3} \quad (16)$$

The accuracy of this approximation was tested by solving numerically the integral of Eq. (15) and comparing this result with that analytically obtained, resulting an error of $\simeq 2.9\%$. In addition, the final analytical solution of Eq. (15)

depends also on the use of the Laurent series approximation for the denominator on the right side of Eq. (15)

$$\frac{1}{\sqrt{\xi^2 - 1}} \simeq \frac{1}{\xi} + \frac{1}{2\xi^3} + \frac{3}{8\xi^5} + \frac{5}{16\xi^7} + \mathcal{O}((1/\xi)^9) \quad (17)$$

Therefore, all the integrals contained in Eq. (15), as well as Eqs. (5)-(6) can be solved in a straightforward way, as shown in Appendix. It is important to emphasize that, in the whole process of analytical calculation, the results for the integrals of Eqs. (5, 6, 7) were confronted with numerical calculations (from *Mathematica*) to check the efficacy of the approximations introduced. As an example, in the graphic of Fig. 2, we compare the continuous line, which is the analytical result for the expectation value of the energy W_+ , with points numerically generated, showing that, despite the large number of approximations, we get a correct analytic expression.

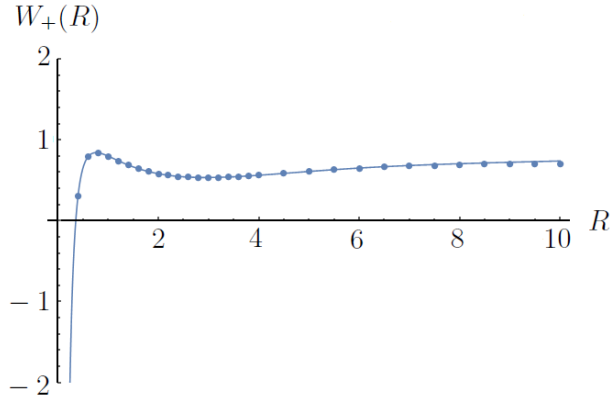


Figure 2: Continuous line is the plot of W_+ function given by Eq. (4) and the dots are some of the numerical results for the same expression.

4. Numerical results

In order to investigate whether the probability of having a μ CF in 2D can be bigger than the corresponding prediction in a 3D system or not, we will compute three different physical quantities:

1. the probability that the nuclei are very close together, namely with a relative distance of the order of 10 fm ($\sim 0.04a_0^*$) [42];

2. the transmission coefficient for having a tunnelling effect from the second well (that on the right of Fig. 2) to the well on the left;
3. the mean distance between the two nuclei in 2D which should be compared with the 3D prediction.

All the calculations done in this section was made using the Numerov method [40] in a program developed by the authors using the C++ language and the CERN/ROOT package, and the graphics were made by running *Mathematica Software*.

Since we want to compare our 2D result with their three-dimensional analogous, we start solving numerically the following equation, Eq. (18), describing the μ CF in 3D given by reference [41]:

$$\left[\frac{d^2}{d\rho^2} + \left(\varepsilon - \frac{\mu}{m_3} \left(W_{\pm}^{3D} + \frac{2}{\rho} \right) \right) \right] u(\rho) = 0 \quad (18)$$

with the 3D expected value of energy W_{\pm}^{3D} being

$$W_{\pm}^{3D} = -\frac{2}{\rho} + \left[-1 + \frac{2}{\rho} + \left(\frac{-\frac{2}{\rho} + 2 \left(\frac{1}{\rho} + 1 \right) e^{-2\rho} \mp 2(1 + \rho)e^{-\rho}}{1 \pm \left(1 + \rho + \frac{\rho^2}{3} \right) e^{-\rho}} \right) \right] \quad (19)$$

A comparison between the effective potential $V_{\text{eff}}^{(3D)}$ and the $V_{\text{eff}}^{(2D)}$, respectively given by Eqs. (8) and (18), considering only the W_+ contribution, is presented in Fig. 3.

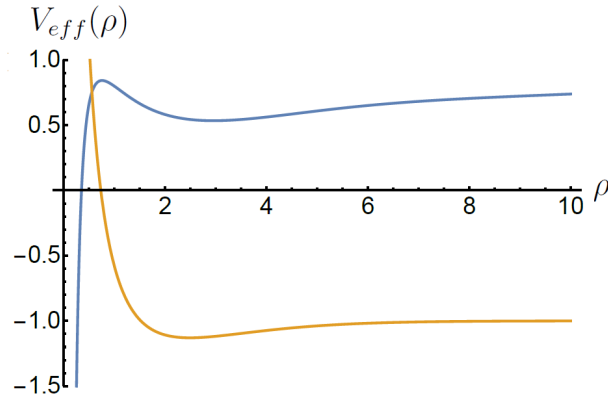


Figure 3: Effective potential in 2D (blue) and 3D (orange) in arbitrary units, for the case $\ell = 0$.

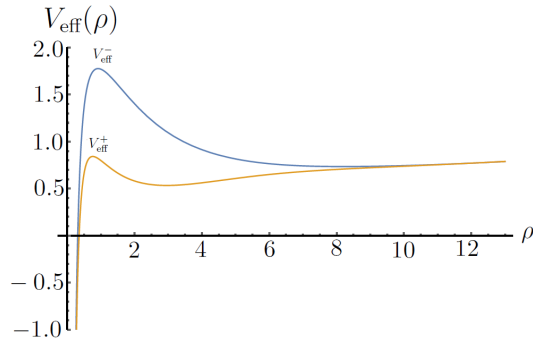


Figure 4: Effective potentials in 2D. One corresponds to W_+ choice (orange), for which we have a second well ($1 \lesssim \rho \lesssim 6$), and the other to W_- (blue), both in arbitrary units, for the case $\ell = 0$, and $\mu/m_3 = 1$.

One should remember that, in 3D, only the effective potential corresponding to W_+ has a minimum energy, *i.e.*, defines a confining well. This is usually attributed to the fact that the even wave function ψ_+ used to compute the mean value energy W_+ maximizes the electron (or muon) probability density between the two nuclei, thereby reducing their mutual electrostatic repulsion. In 2D we have shown that a quite analogous behavior is still valid. The only qualitative difference (for $\ell = 0$) is that now we have also for W_- the same kind of a very deep well for very small ρ values (Fig. 4).

The graphics for wave functions for several molecules in the ground state we are considering are shown in Fig. 5, and are in agreement with those of Ref. [42].

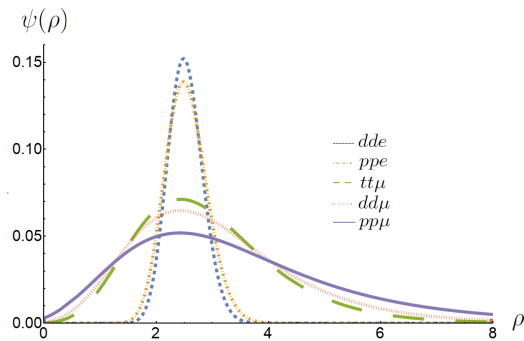


Figure 5: Ground state wave function for different molecules. From the biggest maximum to the lower one we have, respectively: dde , ppe , $tt\mu$, $dd\mu$ and $pp\mu$.

We can now present the solutions of Eq. (8) for different molecules inside the well that goes to $-\infty$, considering just the W_+ contribution. In Fig. 6 the square of the wave functions of the muonic molecules are plotted for the quantum number $\ell = 0$.

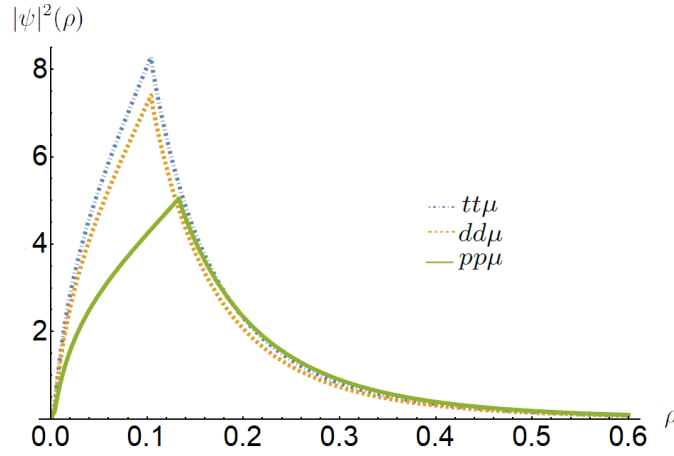


Figure 6: Squared wave functions in 2D for the muonic molecules with the quantum number $\ell = 0$; from the top to the bottom we have: $tt\mu$, $dd\mu$ and $pp\mu$ molecules. The units of ρ axis is in modified Bohr radius units ($a_0^* \simeq \frac{a_0}{206}$).

In Fig. 7 the square of wave functions for dde molecule is shown only for the case $\ell = 0$.

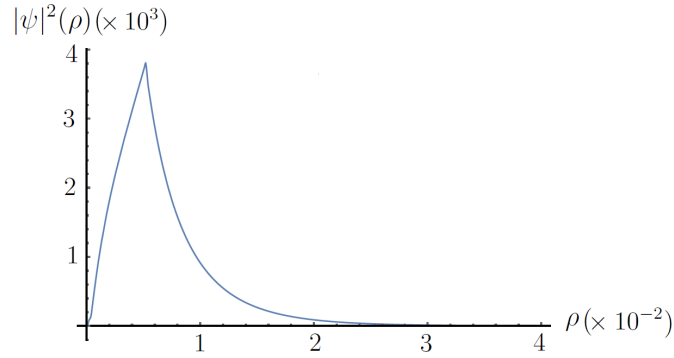


Figure 7: Squared wave functions in 2D for the electronic molecule (dde) with the quantum number $\ell = 0$, the ρ axis is in Bohr radius units (a_0).

The next step was to compute the wave functions inside the second potential

well, as shown in Fig. 8.

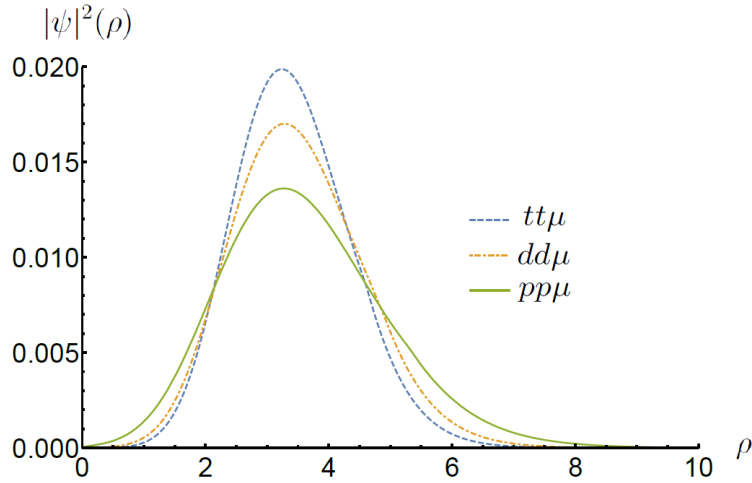


Figure 8: Squared wave functions in 2D for different muonic molecules, for $\ell = 0$. From the top to the bottom, $tt\mu$, $dd\mu$ and $pp\mu$.

The energies, ε , of the muonic molecules corresponding to the wave functions calculated above are given in Table 3.

Table 3: ε value for different muonic molecules. The first region denotes the infinity well for which there is only one energy state, and the second region corresponds to the small well. Also the 3D energy results are given

Molecule	ε		
	2D first region	2D second region	3D
$pp\mu$	-0.9338	3.193	-4.596
$dd\mu$	-2.752	5.846	-9.377
$tt\mu$	-5.836	8.516	-14.2

Our 3D results can be compared to those found in Ref. [42]. We have to be cautious in this comparison, since the molecular reduced mass was not properly taken into account in that paper. In addition, we should express our results for

the energy values in Ry*. Doing so, we reproduce those values within an error of 1.9% for $pp\mu$, 2.5% for $dd\mu$ and 3.3% for $tt\mu$ energies. If we do not take into account the problem involving the reduced masses, the errors are even smaller. All the 2D comparisons will be left to Section 5.

Still inside the first topic enumerated at the beginning of this Section, we can finally calculate the fusion rate, supposing it is proportional to the probability of finding the two nuclei very close together. Following Ref. [42], we chose to calculate this probability for a internuclear separation between 0 and 10 fm ($\simeq 0.04 a_0^*$). This reasonable choice is quite arbitrary but convenient in order to facilitate the comparison of our results with those of Ref. [42].

In general, the probability of a particle inside a region limited by points a and b in 3D is given by

$$\int_a^b |\psi(\rho)|^2 \rho^2 d\rho \quad (20)$$

and, in 2D, is given by

$$\int_a^b |\psi(\rho)|^2 \rho d\rho \quad (21)$$

As already said, all probabilities were calculated from zero to $0.04 a_0^*$ for the muonic molecules and from zero to $0.04 a_0$ for the electronic molecules. These predictions are arranged in the Table 4.

Table 4: Theoretical predictions for the 3D and 2D probabilities of finding the molecules with a small inter nuclear separation is of the order of 10 fm or less. Also the ratios between two- and three-dimensional predictions are given here

Molecule	2D Probability	3D Probability	Ratio (2D/3D)
$pp\mu$	9.3×10^{-3}	2.9×10^{-9}	3.2×10^6
$dd\mu$	1.6×10^{-2}	1.2×10^{-10}	1.3×10^8
$tt\mu$	7.1×10^{-2}	8.2×10^{-12}	1.8×10^9
dde	4.56×10^{-6}	1.7×10^{-88}	2.7×10^{82}

In Ref. [42] the authors defined the fusion rate Λ as a quantity proportional to the probability density (and not the probability), *i.e.*,

$$\Lambda \propto |\psi(\rho)|^2$$

With this definition, they found that the relative fusion rate $\lambda \equiv \Lambda^{2D}/\Lambda^{3D}$, for $\rho = 0.04$, is much smaller than what is found in the present paper. Indeed, they found $\lambda = 350$ for $pp\mu$, $\lambda = 1\,530$ for $dd\mu$ and $\lambda = 5\,620$ for $tt\mu$, to be compared with the respective values of the right column of Table 4. For $tt\mu$ molecule, our prediction is 3×10^5 times bigger than the previous result. We will turn back to this point in the concluding remarks.

The second subject we intend to investigate here is how the tunnelling coefficient (T) changes from going from a 3D to a 2D system.

From Eq. (8), the transmission coefficient for a particle tunnelling through a potential barrier, in dimensionless unity, is [44]

$$\exp\left(-2 \int_{\rho_1}^{\rho_2} d\rho \sqrt{V(\rho) - \varepsilon}\right) \quad (22)$$

where $V(\rho) = \frac{\mu}{m_3} [-\ln \rho + W_{\pm}] + \frac{(\ell^2 - \frac{1}{4})}{\rho^2}$, and ρ_1 and ρ_2 are the two classical turning points for the potential barrier. Eq. (22) gives us a semi-classical estimation for the tunnelling coefficients (T) for the 2D and the 3D cases, as shown in the Table 5.

Table 5: Tunnelling coefficients (T) for the 2D and the 3D cases, calculating with Eq. 22 for different molecules

Molecule	$T(2D)$	$T(3D)$
$pp\mu$	1.56×10^{-2}	1.92×10^{-5}
$dd\mu$	8.03×10^{-4}	1.73×10^{-7}
$tt\mu$	9.28×10^{-5}	4.53×10^{-9}

A direct inspection of the results shown in Table 5 confirms what is well known, *i.e.*, the transmission coefficient is inversely proportional to the nuclei reduced mass. Indeed, $T(pp\mu) > T(dd\mu) > T(tt\mu)$. However, the biggest enhancement of the fusion rate in going from a 3D to a 2D system is found for the $tt\mu$ ionized molecule. If we define, for each molecule M , a parameter $\tau_M \equiv T_M^{2D}/T_M^{3D}$ as the relative factor expressing this enhancement, we get: $\tau_{pp\mu} \simeq 0.8 \times 10^3$, $\tau_{dd\mu} \simeq 4.6 \times 10^3$ and $\tau_{tt\mu} \simeq 2.0 \times 10^4$. Thus, independent of

the kind of molecule we are considering the probability of having a tunnelling effect always increases by going from 3D to 2D.

So, we can safely conclude that the biggest improvement of the fusion rate due to the tunnelling comes out from the $tt\mu$ molecule.

The tunnelling coefficient was not calculated in Ref. [42], where the author limited themselves to argue that the tunnelling is favoured in 2D since in 2D the size of any molecules is smaller than in 3D, as commented later.

The last topic we would like to consider here is the comparison between the predictions for the mean molecular size in 3D e 2D. These sizes can be calculated, respectively, by the following equations:

$$\langle \rho \rangle = \int_0^\infty |\psi(\rho)|^2 \rho^3 d\rho \quad (23)$$

and

$$\langle \rho \rangle = \int_0^\infty |\psi(\rho)|^2 \rho^2 d\rho \quad (24)$$

The numerical results for these expressions are given in Table 6.

Table 6: Mean molecular sizes in 2D and in 3D cases

Molecule	$\langle \rho \rangle_{2D}$	$\langle \rho \rangle_{3D}$
$pp\mu$	4.11222	4.07055
$dd\mu$	3.84134	3.42082
$tt\mu$	3.68447	3.20174

Notice that, for the same molecule, the values are comparable, indicating that for a given positive energy corresponding to the wave functions previously calculated for the second well (Fig. 8), the mean molecular size is quite independent on space dimensionality. Anyway, in both 2D and 3D the radius decreases as the nuclei masses increase.

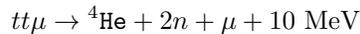
Here a significant difference between our predictions and those of Ref. [42] was found. In fact, although we found that the mean size of the molecule practically do not depend on the space dimensionality, in Ref. [42] the authors claimed that the equilibrium distance between the two nuclei (which is not exactly the

same as the mean size), in 2D, is estimated to be 1/4 of the corresponding value in 3D.

5. Concluding remarks

The overall conclusion of this paper is that the rates for μCF is strongly enhanced in a 2D quasi-adiabatic model, if the two nuclei inside the ionized muonic molecules are in a s -state ($\ell = 0$). From a practical point of view, we have enlightened the question in what extent the fusion rate increases from passing from a 3D model to a 2D one. Indeed, Table 4 summarizes the enhancement factor for each one of the molecules we have considered. The smaller value for the relative ratio ($2D/3D$) is 3.2×10^6 for $pp\mu$ and the larger one is 1.8×10^9 for $tt\mu$. In complement, the tunnelling factor, in the case of $pp\mu$, increases by a factor $\tau \simeq 790$, while for $tt\mu$ we got $\tau \simeq 2 \times 10^4$.

In summary, from the three types of ionized molecules we have studied, we have found that the most favorable μCF corresponds to the molecule $tt\mu$, from which one expect a nuclear reaction of the type



As already said, we hope to treat ionized molecules with different nuclei, like $dt\mu$ [26, 45, 46] (in this case, for each fusion 17 MeV of energy are released), in a future publication.

Now, from the theoretical point of view, we can argue what is the most crucial reason for these results. This question makes sense if we remember that, in passing from a 3D model to a 2D model, two qualitatively different features are changed: the first, which is essentially a geometric factor, is the centrifugal potential $\ell(\ell + 1)/r^2$ in 3D which is replaced by $(\ell^2 - 1/4)/r^2$ in 2D, and the dynamical potential between charge particles changes from $1/r$ to $\ln(r)$.

Therefore, we can wonder whether our predictions and their comparison with others can shed light on what actually made the 2D model for the μCF so peculiar.

First of all, we stress the unique features of the effective potential energy (V_{eff}) when the angular momentum between the two molecular nuclei is zero ($\ell = 0$). Only in this case V_{eff} has two distinct wells: a very sharp one, going to $-\infty$, when $\rho \rightarrow 0$ and showing on the right side a maximum around $\rho \simeq 0.5$, and a second well that goes from this maximum up to $\rho \simeq 5$. The existence

of such a maximum facilitates the tunnelling effect when compared with the other V_{eff} curves for $\ell = 1, 2, 3, \dots$ (Fig. 9). Indeed, increasing the value of ℓ , the abscissa of the minimum of the remaining well goes to the right and the ordinate increases, as shown in Fig. 9, for $\ell = 1$. This means that the tunnelling coefficient decreases whenever ℓ increases and one should have a bigger mean value of ρ .

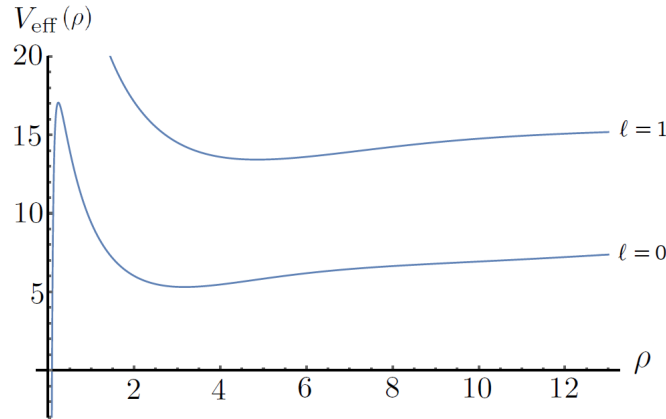


Figure 9: Sketch of two effective potentials related to W_+ in 2D, for $\ell = 0$ and $\ell = 1$.

Secondly, the results summarized in Table 4 show that the probability of finding the two nuclei in the region $0 \lesssim \rho \lesssim 0.04$ (which, by hypothesis, is a requirement for fusion startup) is much higher than the equivalent probability in 3D.

Finally, let us make a comment comparing the effect of the $e \rightarrow \mu$ substitution inside the molecule *versus* the effect of dimensional reduction from 3D to 2D.

Looking at Table 4, one realizes, as expected, that the replacement of the electron inside the ionized molecule by a muon gives rise to a higher probability of fusion. But what to say about the effect of having reduced the dimension of the system?

Our numerical program can be easily adapted for molecules with electrons. In particular, we have calculated the probability of fusion for dde in 2D and 3D. The results are exhibit in Table 4. We can see that, for dde , the 2D probability is 3.7×10^4 times bigger than the probability of fusion for the molecule $dd\mu$ in 3D. We also have a 2D probability fusion for $dd\mu$ 1.3×10^8 times bigger

than the 3D probability for the same molecule. These results suggest that if one keep the electron inside the molecule and only reduces space dimensionality from 3 to 2 the probability of fusion is still significantly increased (by a factor 10^4 in this case) with respect to the situation where the space dimensionality is maintained and the electron is replaced by a muon. However, substituting $e \rightarrow \mu$ and, at the same time, reducing the space dimensionality gives us a gain of $(10^4)^2$. Unfortunately, Ref. [42] do not give us a prediction for the fusion probability in the case of dde molecule in 2D computed with the $1/r$ Ansatz, instead of $\ln(r)$.

We hope that this work could contribute to a better understanding of how a muon-catalyzed fusion actually works in two dimensions, and that the complete planar multi-interaction fusion process could be investigated in a near future, especially for $tt\mu$ and $dt\mu$.

Acknowledgments

We are grateful to Edgardo Cheb-Terrab for his help concerning the use of *Maple 17* and for fruitful suggestions, as well as to Diógenes Galetti for reading a preliminar version of this paper and for some critical remarks. This study was financed in part by the Coordenação de Aperfeiçoamento de Pessoal de Nível Superior – Brazil (CAPES), Finance Code 001. AT thanks CNPq of Brazil for a research grant.

References

- [1] Lattes, Cesare Mansueto Giulio and Occhialini, Giuseppe Paolo Stanislao and Powell, Cecil Frank, Observations on the tracks of slow mesons in photographic emulsions, *Nature*, **160**, n. 4067, 486-492, 1947.
- [2] Frank, F.C., Hypothetical alternative energy sources for the “second meson” events, *Nature*, **160**, 525-527, 1947.
- [3] Sakharov, A.D., Passive mesons (in Russian “Passivnyie mezony”) *Report of Lebedev Physical Institute of the Academy of Sciences of USSR* (1948). English translation in *Muon Catalyzed Fusion*, **4**, 235-239, 1989.
- [4] Ponomarev, L.I., Muon catalysed fusion, *Contemporary Physics*, **31**, n. 4, 219-245, 1990.

- [5] Balin, D.V. and Ganzha, V.A. and Kozlov, S.M. and Maev, E.M. and Petrov, G.E. and Soroka, M.A. and Schapkin, G.N. and Semenchuk, G.G. and Trofimov, V.A. and Vasiliev, A.A. and others, High precision study of muon catalyzed fusion in D_2 and HD gas, *Physics of Particles and Nuclei*, **42**, n. 2, 185-214, 2011.
- [6] Alvarez, Luis W. and Bradner, H. and Crawford Jr, F.S. and Crawford, J.A. and Falk-Vairant, P. and Good, M.L. and Gow, J.D. and Rosenfeld, A.H. and Solmitz, F. and Stevenson, M.L. and Ticho, H.K. and Tripp, R.D., Catalysis of nuclear reactions by μ mesons, *Physical Review*, **105**, n. 3, 1127-1128, 1957.
- [7] Matveenko, A.V. and Ponomarev, L.I., Calculation of the $p\mu + \text{He}^{++}$ reaction, *Zhurnal Eksperimental'noj i Teoreticheskoy Fiziki*, **63**, n. 1, 48-52, 1972
- [8] Ponomarev, L.I. and Puzynin, I.V. and Puzynina, T.P., Continuous analog of Newton's method as applied to the calculation of the binding energy of mesic molecules, *Journal of Computational Physics*, **13**, n. 1, 1-14, 1973.
- [9] Nagamine, K. and Ponomarev, L.I., Recent progress in muon catalyzed fusion, *Nuclear Physics A*, **721**, C863-C866, 2003.
- [10] Jones, Steven Earl, Muon-catalysed fusion revisited, *Nature*, **321**, n. 6066, 127-133, 1986.
- [11] Jackson, John David, Catalysis of nuclear reactions between hydrogen isotopes by μ^- mesons, *Physical Review*, **106**, n. 2, 330-339, 1957.
- [12] Dzhelepov, V.P. and Ermolov, P.F. and Moskalev, V.I. and Fil'Chenkov, V.V., Catalysis by Negative Muons of the Nuclear Reactions $d\mu + p \rightarrow \text{He}^3 + \mu^-$ and $d\mu + d \rightarrow t + p + \mu^-$ and Formation of the Molecules $pd\mu$ and $dd\mu$ in Gaseous Hydrogen, *Soviet Journal of Experimental and Theoretical Physics*, **23**, 820-831, 1966.
- [13] Vesman, E.A., Concerning One Possible Mechanism of Production of the Mesic-molecular Ion $(dd\mu)^+$, *Soviet Journal of Experimental and Theoretical Physics Letters*, **5**, 91-93, 1967.
- [14] Breunlich, W.H. and *et al.*, Muon-Catalyzed $D - T$ Fusion at Low Temperature, *Physical Review Letters*, **58**, n. 4, 329-332, 1987.

- [15] Bystritsky, V.M. and *et al.*, Experimental study of μ -atomic and μ -molecular processes in a pure helium and deuterium-helium mixtures, *Physical Review A*, **71**, 0327231-12, 2005.
- [16] Jandel, M. and Danos, M. and Rafelski, J., Active target production of muons for muon-catalyzed fusion, *Physical Review C*, **37**, n. 1, 403-406, 1988.
- [17] Ackerbauer, P. and Werner, J. and Breunlich, W.H. and Cargnelli, M. and Fussy, S. and Jeitler, M. and Kammel, P. and Marton, J. and Scrinzi, A. and Zmeskal, J. and others, Experimental investigation of muon-catalyzed *dt* fusion at cryogenic temperatures, *Nuclear Physics A*, **652**, n. 4, 311-338, 1999.
- [18] Holmlid, Leif, Existing Source for Muon-Catalyzed Nuclear Fusion Can Give Megawatt Thermal Fusion Generator, *Fusion Science and Technology*, **75**, n. 3, 208-217, 2019, and references therein.
- [19] Petitjean, C., Progress in muon catalyzed fusion, *Nuclear Physics A*, **543**, n. 1-2, 79-97, 1992.
- [20] Petrov, Yu.V., Muon catalysis for energy production by nuclear fusion, *Nature*, **285**, n. 5765, 466-468, 1980.
- [21] Breunlich, W. H., Muon catalyzed fusion, *Nuclear Physics A*, **508**, 3-15, 1990.
- [22] Rafelski, J. and Jones, S.E., Cold Nuclear Fusion, *Scientific American*, **257**, n. 1, 84-89, 1987.
- [23] Scrinzi, A. and *et al.*, Muon-catalyzed *dd* fusion between 25 and 150 K: Theoretical analysis, *Physical Review A*, **47**, n. 6, 4691-4704, 1993.
- [24] Bogdanova, L.N. and *et al.*, The Probability of muon sticking to helium in the muon-catalyzed fusion $dt\mu \rightarrow \mu\text{-}^4\text{He} + \text{n}$, *Nuclear Physics A*, **454**, 652-668, 1986.
- [25] Révai, J. and Zubarev, A.L. and Higer, L.Ya. and Belyaev, V.B., Effect of the nuclear *d-t* resonance on muon-sticking in μ -catalyzed fusion, *Physical Review A*, **43**, n. 9, 4611-4616, 1991.

- [26] Jones, S.E. and *et al.*, Observation of unexpected density effects in muon-catalyzed *d-t* fusion, *Physical Review Letters*, **56**, n. 6, 588-591, 1986.
- [27] da Cunha Lima, I.C. and da Silva, A. Ferreira and Fabbri, M. and Troper, A., Variation of the Fusion Rate of the Deuterium Molecule in an Effective Medium, *Modern Physics Letters B*, **7**, n. 13 & 14, 949-952, 1993.
- [28] Geim, A.K. and Novoselov, K.S. and Lastauthor, E., The rise of graphene, *Nature*, **6**, 183-191, 2007.
- [29] Geim, A.K., Graphene: status and prospects, *Science*, **324**, 1530-1534, 2009.
- [30] Zhang, Y. and *et al.*, Direct Observation of a widely tunable bandgap in bilayer graphene, *Nature*, **459**, 820-823, 2009.
- [31] Laughlin, R.B., Direct Observation of a widely tunable bandgap in bilayer graphene, *Physical Review Letters*, **50**, 1395-1398, 1983.
- [32] Prange, R.E. and Girvin, S.M., *The Quantum Hall Effect*, New York, Springer, 2012.
- [33] Eveker, K. and *et al.*, Direct Observation of a widely tunable bandgap in bilayer graphene, *American Journal of Physics*, **58**, 1183-1192, 1990.
- [34] Eveker, K. and *et al.*, Exact e-e (exchange) correlations of 2-D quantum dots in magnetic field: Size extensive $N = 3, 4, \dots$, 'n'-electron systems via multi-pole expansion, *Physica E: Low-dimensional Systems and Nanostructures*, **88**, 26-43, 2017.
- [35] Sadeghi, E. and M. Moradi Lm, Exchange and Coulomb interactions of two electrons in double ellipsoidal quantum dots, *Physica E: Low-dimensional Systems and Nanostructures*, **70**, 141-145, 2015.
- [36] Lapidus, I. Richard, One- and two-dimensional hydrogen atoms, *American Journal of Physics*, **49**, 807-807, 1981.
- [37] Caruso, F. and Oguri, V. and Silveira, F., How the inter-electronic potential Ansätze affect the bound state solutions of a planar two-electron quantum dot model, *Physica E: Low-dimensional Systems and Nanostructures*, **105**, 182-185, 2019.

- [38] Caruso, F. and Oguri, V. and Silveira, F., Numerical Solutions for a Two-dimensional Quantum Dot Model, *Brazilian Journal of Physics*, **49**, n. 3, 432-437, 2019.
- [39] Numerov, Boris Vasil'evich, A Method of Extrapolation of Perturbations, *Monthly Notices of the Royal Astronomical Society*, **84**, 592-601, 1924.
- [40] Caruso, Francisco and Oguri, Vitor, Numerov numerical method applied to the Schrödinger equation, *Revista Brasileira de Ensino de Física*, **36**, n. 2, 1-7, 2014.
- [41] Park, D., *Introduction to the Quantum Theory*, 3rd edition, Mineola, NY, Dover, 2005.
- [42] da Cunha Lima, I.C. and Fabbri, M. and da Silva, A. Ferreira and Troper, A., Calculation of ground-state energies of muonic molecules of hydrogen isotopes confined to a two-dimensional region, *Physical Review A*, **41**, n. 7, 4049-4051, 1990.
- [43] Bateman, H. and Erdélyi, A., *Higher Transcendental Functions, vol. 1*, New York, McGraw-Hill, 1953.
- [44] Razavy, M., *Quantum Theory of Tunneling*, Singapore, World Scientific, 2003.
- [45] Gershtein, S.S. and Ponomarev, L.I., μ^- Meson Catalysis Of Nuclear Fusion In A Mixture Of Deuterium And Tritium, *Physics Letters B*, **76**, n. 1, 80-82, 1977.
- [46] Kino, Y. and Harston, M.R. and Shimanura, I. and Armour, E.A.G. and Kaminura, M., Normalization of the asymptotic form of three-body $(dt\mu)^+$ and $(dd\mu)^+$ wave functions, *Physical Review A*, **52**, n. 1, 870-873, 1995.

6. Appendix

The complete result for the *overlap integral* Δ can be expressed in terms of incomplete gamma functions, $\Gamma(s, \rho)$, and of the modified Bessel function of the second kind, $K_3(\rho)$, as follows:

$$\begin{aligned} \Delta &= \frac{\rho^3}{2\pi} \left\{ \frac{\pi}{4} K_3(\rho) + \frac{\pi}{64} \left[9\rho \Gamma(-1, \rho) + \frac{23}{4} \rho^3 \Gamma(-3, \rho) + \right. \right. \\ &\quad \left. \left. + \frac{32}{8} \rho^5 \Gamma(-5, \rho) + \frac{105}{32} \rho^7 \Gamma(-7, \rho) + \frac{25}{68} \rho^9 \Gamma(-9, \rho) \right] \right\} \end{aligned} \quad (25)$$

To solve Eq. (6), first let's write it in prolate coordinate system

$$\begin{aligned} \mathcal{E} &= \frac{\rho^3}{4\pi} \left\{ 2 \ln\left(\frac{\rho}{2}\right) \int_{-1}^1 \frac{d\eta}{\sqrt{1-\eta^2}} \int_1^\infty d\xi \frac{(\xi^2 - \eta^2)^{\frac{3}{2}} e^{-\rho\xi}}{\sqrt{\xi^2 - 1}} + \right. \\ &\quad + \int_{-1}^1 \frac{d\eta}{\sqrt{1-\eta^2}} \left[\int_1^\infty d\xi \frac{\ln(\xi + \eta)(\xi^2 - \eta^2)^{\frac{3}{2}} e^{-\rho\xi}}{\sqrt{\xi^2 - 1}} + \right. \\ &\quad \left. \left. + \int_1^\infty d\xi \frac{\ln(\xi - \eta)(\xi^2 - \eta^2)^{\frac{3}{2}} e^{-\rho\xi}}{\sqrt{\xi^2 - 1}} \right] \right\} \end{aligned}$$

The trick here to find the analytical solution of the second and the third integrals of the last expression for \mathcal{E} is to expand each one in a Taylor series in the variable ξ around $\eta = 0$ up to the sixth order using *Maple 17* software, according to which

$$\begin{aligned} \int_1^\infty \frac{\ln(\xi \pm \eta)(\xi^2 - \eta^2)^{\frac{3}{2}} e^{-\rho\xi}}{\sqrt{\xi^2 - 1}} d\xi &\simeq \int_1^\infty \frac{\ln(\xi) e^{-\rho\xi} \xi^3}{\sqrt{\xi^2 - 1}} d\xi + \\ &\mp g_1 \eta + g_2 \eta^2 \mp g_3 \eta^3 + g_4 \eta^4 \pm g_5 \eta^5 + \mathcal{O}(\eta^6) \end{aligned}$$

with

$$\begin{aligned} g_1 &= \frac{1}{\rho} G_{1,3}^{2,1} \left(\frac{\rho^2}{4} \middle| \begin{matrix} 0 \\ \frac{1}{2}, -\frac{1}{2}, 1 \end{matrix} \right) \\ g_2 &= -\frac{1}{2} \int_1^\infty \left[\frac{3 \ln(\xi) e^{-\rho\xi} \xi}{\sqrt{\xi^2 - 1}} + \frac{e^{-\rho\xi} \xi}{\sqrt{\xi^2 - 1}} \right] d\xi \\ g_3 &= \frac{7}{6} K_0(\rho) \\ g_4 &= \frac{1}{2} \int_1^\infty \left[\frac{3 \ln(\xi) e^{-\rho\xi}}{4\xi \sqrt{\xi^2 - 1}} + \frac{e^{-\rho\xi}}{\xi \sqrt{\xi^2 - 1}} \right] d\xi \\ g_5 &= \frac{3\rho^3}{640} G_{1,3}^{3,0} \left(\frac{\rho^2}{4} \middle| \begin{matrix} 0 \\ -\frac{1}{2}, -1, -\frac{3}{2} \end{matrix} \right) \end{aligned}$$

Whenever necessary, the same Laurent series approximation, Eq. (17), was used, as for the Δ calculation. Here $K_0(\rho)$ is a modified Bessel function of the second kind and $G_{p,q}^{m,n} \left(z \left| \begin{smallmatrix} a_1, \dots, a_n \\ b_1, \dots, b_n \end{smallmatrix} \right. \right)$ denotes the general function called Meijer-G [43].

After a straightforward and long calculation the result can be simplified in such a way that the factor \mathcal{E} depends only on a particular incomplete gamma function and on different Meijer-G functions, *i.e.*,

$$\begin{aligned} \mathcal{E}(\rho) = & \frac{\rho^3}{2048} \left\{ 768 \frac{\Gamma(0, \rho)}{\rho} + 144 G_{2,3}^{3,0} \left(\rho \left| \begin{smallmatrix} 2, 2 \\ 0, 1, 1 \end{smallmatrix} \right. \right) + \right. \\ & + 104 G_{2,3}^{3,0} \left(\rho \left| \begin{smallmatrix} 4, 4 \\ 0, 3, 3 \end{smallmatrix} \right. \right) + 186 G_{2,3}^{3,0} \left(\rho \left| \begin{smallmatrix} 6, 6 \\ 0, 5, 5 \end{smallmatrix} \right. \right) + \\ & \left. + 45 G_{2,3}^{3,0} \left(\rho \left| \begin{smallmatrix} 8, 8 \\ 0, 7, 7 \end{smallmatrix} \right. \right) \right\} \end{aligned} \quad (26)$$

The last integral to be solved is that of Eq. (5), which, in the prolate coordinate system, is:

$$\mathcal{D} = \ln \frac{\rho}{2} + \frac{\rho^3}{2\pi} \int_{-1}^1 \frac{e^{\rho\eta} d\eta}{\sqrt{1-\eta^2}} \int_1^\infty \ln(\xi + \eta) e^{-\rho\xi} \frac{(\xi - \eta)(\xi^2 - \eta^2)}{\sqrt{\xi^2 - 1}} d\xi \quad (27)$$

In this case, the slow convergence in the variable ξ , leads us to take terms up to the seventeenth order of ξ in the Taylor series expansion of the second integral. This choice assures that the analytical result and the numerical one differ from each other just by a factor of the order of 2%. Due to the large number of terms in this expansion we chose not to show them explicitly. As in the previous case, we started using the *Maple 17* software for the expansion of the integral in the variable ξ . Use has also been made of Laurent series expansion whenever necessary. In this case, we were able to obtain an analytical expression for Eq. (27), that depends on the modified Bessel functions of the first and second kind, $I_n(\rho)$ and $K_n(\rho)$, on one incomplete gamma function and on several Meijer-G functions, namely:

$$\begin{aligned}
\mathcal{D}(\rho) &= g_0 + g_1 \frac{\Gamma(0, \rho)}{\rho} + g_2 G_{2,3}^{3,0} \left(\rho \left| \begin{array}{c} -1, -1 \\ -2, -2, 0 \end{array} \right. \right) + \\
&+ g_3 G_{2,3}^{3,0} \left(\rho \left| \begin{array}{c} -2, -2 \\ -3, -3, 0 \end{array} \right. \right) + \\
&+ \sum_{n=1}^7 g_{n+3} G_{2,3}^{3,0} \left(\rho \left| \begin{array}{c} n, n \\ 0, n-1, n-1 \end{array} \right. \right) + \\
&+ \sum_{n=0}^{17} (-1)^n h_n G_{1,3}^{3,0} \left(\frac{\rho^2}{4} \left| \begin{array}{c} 0 \\ -\frac{1}{2}, -\frac{(1+n)}{2}, -\frac{(2+n)}{2} \end{array} \right. \right) \quad (28)
\end{aligned}$$

The explicit form of the g_n e h_n factors are:

$$\begin{aligned}
g_0 &= \ln\left(\frac{\rho}{2}\right) + \frac{\rho^3}{2} \left[[K_0(\rho) + K_1(\rho)] I_1(\rho) - \frac{1}{6} K_0(\rho) I_3(\rho) + \right. \\
&\quad \left. - \frac{3}{2} K_1(\rho) I_2(\rho) \right] - \frac{3}{4} [K_1(\rho) I_1(\rho) + \frac{1}{3} K_0(\rho) I_2(\rho)] \\
g_1 &= -\frac{\rho^3}{4} I_2(\rho) \\
g_2 &= -\frac{\rho^3}{2} I_1(\rho) \\
g_3 &= \frac{\rho^3}{2} I_0(\rho) \\
g_4 &= \frac{\rho^2}{4} [\rho I_1(\rho) - 2I_2(\rho)] \\
g_5 &= -\frac{\rho^2}{16} [\rho I_0(\rho) - 4I_1(\rho)] \\
g_6 &= \frac{\rho^3}{16} I_3(\rho) \\
g_7 &= -\frac{\rho}{32} [\rho I_0(\rho) - 6I_1(\rho)] \\
g_8 &= \frac{\rho^2}{32} [\rho I_1(\rho) - 6I_2(\rho)] \\
g_9 &= -5\rho^2 [I_1(\rho) + \rho I_2(\rho)] \\
g_{10} &= \frac{5\rho^2}{32} [3I_2(\rho) + \rho I_3(\rho)]
\end{aligned}$$

$$h_0 = \frac{11}{192} \rho^3 (\rho^2 + 3) I_2(\rho)$$

$$h_1 = \frac{23}{960} \frac{\rho^4}{2} [(\rho^2 + 15) I_3(\rho) + 2\rho I_4(\rho)]$$

$$\begin{aligned}
h_2 &= \frac{13}{1920} \frac{\rho^4}{2} [5(\rho^2 + 3) I_3(\rho) + (\rho^2 + 5) \rho I_4(\rho)] \\
h_3 &= \frac{59}{26880} \frac{\rho^5}{2} [3(3\rho^2 + 35) I_4(\rho) + (\rho^2 + 15) \rho I_5(\rho)] \\
h_4 &= \frac{83}{107520} \frac{\rho^5}{2} [4\rho^3 I_5(\rho) + (\rho^4 + 42\rho^2 + 105) I_4(\rho)] \\
h_5 &= \frac{37}{129024} \frac{\rho^6}{2} [4(2\rho^2 + 21) \rho I_6(\rho) + [\rho^4 + 98\rho^2 + 945] I_5(\rho)] \\
h_6 &= \frac{143}{1290240} \frac{\rho^6}{2} [(13\rho^4 + 378\rho^2 + 945) I_5(\rho) + \\
&\quad + (\rho^4 + 42\rho^2 + 189) \rho I_6(\rho)] \\
h_7 &= \frac{179}{4055040} \frac{\rho^7}{2} [(19\rho^4 + 1170\rho^2 + 10395) I_6(\rho) + \\
&\quad + \rho(\rho^4 + 94\rho^2 + 945) I_7(\rho)] \\
h_8 &= \frac{73}{4055040} \frac{\rho^7}{2} [12(\rho^2 + 27) \rho^3 I_7(\rho) + \\
&\quad + (\rho^6 + 189\rho^4 + 4455\rho^2 + 10395) I_6(\rho)] \\
h_9 &= \frac{263}{35143680} \frac{\rho^8}{2} [18\rho(\rho^4 + 60\rho^2 + 495) I_8(\rho) + \\
&\quad + (\rho^6 + 345\rho^4 + 16335\rho^2 + 135135) I_7(\rho)] \\
h_{10} &= \frac{311}{98402304} \frac{\rho^8}{2} [5(5\rho^6 + 561\rho^4 + 11583\rho^2 + 27027) I_7(\rho) + \\
&\quad + \rho(\rho^6 + 183\rho^4 + 4455\rho^2 + 19305) I_8(\rho)] \\
h_{11} &= \frac{121}{89456640} \frac{\rho^9}{2} [33(\rho^6 + 191\rho^4 + 7735\rho^2 + 61425) I_8(\rho) + \\
&\quad + \rho(\rho^6 + 333\rho^4 + 15675\rho^2 + 135135) I_9(\rho)] \\
h_{12} &= \frac{419}{715653120} \frac{\rho^9}{2} [24(\rho^4 + 110\rho^2 + 2145) \rho^3 I_9(\rho) + \\
&\quad + (\rho^8 + 564\rho^6 + 47190\rho^4 + 900900\rho^2 + 2027025) I_8(\rho)] \\
h_{13} &= \frac{479}{1871708160} \frac{\rho^{10}}{2} \times \\
&\quad \times [(\rho^8 + 900\rho^6 + 123942\rho^4 + 4504500\rho^2 + 34459425) I_9(\rho) + \\
&\quad + 8\rho(4\rho^6 + 753\rho^4 + 30030\rho^2 + 225225) I_{10}(\rho)] \\
h_{14} &= \frac{181}{1604321280} \frac{\rho^{10}}{2} \times \\
&\quad \times [(41\rho^8 + 12324\rho^6 + 859950\rho^4 + 15315300\rho^2 + 34459425) \times \\
&\quad \times I_9(\rho) + \rho(\rho^8 + 548\rho^6 + 45630\rho^4 + 900900\rho^2 + 3828825) I_{10}(\rho)] \\
h_{15} &= \frac{611}{12192841728} \frac{\rho^{11}}{2} \times \\
&\quad \times [3(17\rho^8 + 7756\rho^6 + 870870\rho^4 + 29238300\rho^2 + 218243025) I_{10}(\rho) + \\
&\quad + \rho(\rho^8 + 876\rho^6 + 119574\rho^4 + 4340700\rho^2 + 34459425) I_{11}(\rho)] \\
h_{16} &= \frac{683}{30482104320} \frac{\rho^{11}}{2} \times \\
&\quad \times [(17403750\rho^4 + 297604125\rho^2 + 654729075 + \\
&\quad + \rho^{10} + 1335\rho^8 + 282450\rho^6) I_{10}(\rho) + \\
&\quad + 40\rho^3(\rho^6 + 297\rho^4 + 20475\rho^2 + 348075) I_{11}(\rho)]
\end{aligned}$$